Mineral Lithotype Identification on the Andrill AND-2A Drillcore, Antarctica by Using Ternary Mineral Rock Physics Templates built from a Self-Consistent Approach

Jaime Meléndez-Martínez[1], Rubén Nicolás-López[2], Oscar C. Valdiviezo-Mijangos[3*]

Resumen

En este trabajo, los valores de densidad volumétrica húmeda ρ_{WBD} y de velocidad onda compresional V_P obtenidas a lo largo del núcleo de perforación AND-2A son graficados sobre plantillas ternarias de física de rocas (Rock Physics Templates, RPTs) construidas a partir de un modelo micromecánico autoconsistente (Self-Consistent, SC) con el fin de determinar las tendencias en las propiedades elásticas del núcleo que permitan ayudar a identificar los litotipos minerales y en consecuencia identificar también las características litológicas presentes a lo largo de los 1138 m. de longitud del núcleo. Las propiedades elásticas de los tres minerales dominantes presentes en el núcleo de perforación (arcillas mixtas, cuarzo y calcita); así como el fluido que satura su espacio poroso (salmuera) se utilizaron como insumos del modelo autoconsciente. La litología interpretada es también comparada con la que se obtiene a partir del análisis de los valores de ρ_{WBD} y V_P utilizando gráficos cruzados de densidad-velocidad de tipo Gardner. Los resultados que se obtienen usando los métodos SC y de Gardner concuerdan con las principales litologías presentes a lo largo del núcleo AND-2A reportadas en la literatura científica. Nuestros resultados también son consistentes con la descripción litológica de seis muestras de roca obtenidas a diferentes profundidades del núcleo AND-2A. Estos resultados sugieren que las predicciones del método autoconsistente podrían ser útiles para ayudar a identificar litología en perforaciones científicas en donde las propiedades elásticas a lo largo de la pared del pozo de perforación podrían existir en intervalos en los que no se recuperaron muestras del núcleo de perforación.

Además, incluso cuando las propiedades físicas elásticas se obtienen a través de mediciones en núcleos, el método autoconsistente también es útil porque la litología a veces puede ser difícil de determinar solamente a partir del análisis visual; de modo que el estudio de las propiedades físicas del núcleo puede proporcionar mayor información.

Palabras clave: plantillas de física de rocas, método auto consistente, sedimentos antárticos, núcleo de perforación AND-2A y relación de Gardner.

Corresponding author at ovaldivi@imp.mx

[1]*Instituto Mexicano del Petróleo*
 Eje Central Lázaro Cárdenas Norte 152, Gustavo A. Madero,
 San Bartolo Atepehuacan, 07730 Mexico City, Mexico.
 Jaime Meléndez-Martínez, email: jaimem@imp.mx

[2]*Instituto Mexicano del Petróleo*
 Eje Central Lázaro Cárdenas Norte 152, Gustavo A. Madero,
 San Bartolo Atepehuacan, 07730 Mexico City, Mexico.
 División de estudios de Posgrado de la Facultad de Ingeniería,

Universidad Nacional Autónoma de México.
Ciudad Universitaria, Delegación Coyoacán, 04510, Mexico City, Mexico.
Rubén Nicolás-López, email: rnlopez@imp.mx

[3]*Instituto Mexicano del Petróleo*
 Eje Central Lázaro Cárdenas Norte 152, Gustavo A. Madero,
 San Bartolo Atepehuacan, 07730 Mexico City, Mexico.
 Instituto Politécnico Nacional, ESIA Ticomán
 Calz. Ticomán 600, San José Ticomán, Gustavo A. Madero, 07340 México City, Mexico

ABSTRACT

In this work, wet bulk density ρ_{WBD} and compressional wave velocity V_P core log data obtained along the AND-2A drillcore are plotted on density-velocity ternary mineral Rock Physics Templates (RPTs) built from a Self-Consistent (SC) micromechanics modelling with the purpose to determine data trends that allow us to assist in identifying mineral lithotypes and lithological features throughout the 1138 m length of the drillcore. The elastic properties of the three dominant minerals present in the drillcore (mixed clays, quartz, and calcite) and the pore-filling fluid (brine) were used as input data for the SC model. The interpreted lithology is then compared to that obtained from the analysis of the AND-2A drillcore ρ_{WBD} and V_P log data using Gardner type density-velocity cross plots. Results from both the SC and Gardner methods are in good agreement with the main lithologies present in the AND-2A drillcore already reported in the scientific literature. Our findings also agree well when compared to the lithological description of six selected rock samples obtained at different depths on the AND-2A drillcore. These results suggest that the proposed SC approach could be helpful to assist to identify lithology in scientific drill holes where downhole elastic properties may exist over intervals where portions of the drillcore were not recovered. Furthermore, even when elastic property data sets come from measurements on cores, the SC approach is likewise useful because, from visual analysis alone, lithology can sometimes be difficult to determine, and additional information from the analysis of the elastic properties may provide more insight.

KEY WORDS: rock physics templates, self-consistent method, Antarctic sediments, AND-2A drillcore and Gardner´s relationship.

INTRODUCTION

Antarctica has endured repeated ice sheets since the Cenozoic, while continuous glaciations have been experienced in the Northern Hemisphere since the beginning of the Pliocene (Wilson *et al.*, 2012). Therefore, broad areas are now covered with glacially deposited sediments. Populations settled in such areas, mainly in the northern hemisphere, obtain water from, and place waste in these sediments (Stephenson *et al.*, 1988). Consequently, knowledge of the different mineral lithotypes, and therefore, the lithology present in these geological materials is important for both the development of engineering projects and for geophysical assessments. Despite their significance, there is a scarcity of information about their lithological features since such sediments are frequently located in remote areas (Brink & Jarrard, 1998; Niessen & Jarrard, 1998; Niessen *et al.*, 1998) making it difficult to obtain appropriate geophysical data sets used to describe the lithology of these sediments. In this sense, we make use of the existence of density and velocity core log data obtained from the AND-2A to assist in identifying lithology using ternary Rock Physics Templates. RPTs are built using rock physics modelling with the purpose of relating the physical properties of rocks to their particular geological features and to identify fluid content (Close *et al.*, 2012). Here, we attempt to use ternary mineral RPTs to relate the AND-2A drillcore's elastic properties to mineral lithotypes (mineral assemblage facies), and then to lithology. The AND-2A drillcore was obtained by the ANtartic DRILLing project (ANDRILL) as part of the Southern McMurdo Sound Project (SMS) (Florindo *et al.*, 2008-2009). Drilling started over a sea ice platform (8.5 m thick) while lying on the surface of a 380 m seawater column and finished at 1138 meters beneath the seafloor [mbsf] (Wonik *et al.*, 2008-2009). The elastic properties corresponding to the AND-2A drillcore that are used in this contribution are the ρ_{WBD} and the V_P core log data, while the ternary mineral diagrams

are generated from a micromechanics SC modelling using the scheme implemented by Sabina and Willis (1988). This SC scheme seeks to compute the effective elastic properties of a heterogeneous isotropic rock composite assuming that the composite contains an isotropic mineral matrix embedded with *n* isotropic inclusions (minerals and the fluid that saturates the porous space of the rock). As such, in our case, the heterogeneous isotropic composite represents the AND-2A drillcore. This SC approach has been already implemented to calculate the elastic properties of gas-oil shale systems (Valdiviezo-Mijangos & Nicolás-Lopez, 2014; Nicolás-López & Valdiviezo-Mijangos, 2016; Lizcano-Hernández *et al.*, 2018; Nicolás-López *et al.*, 2020; López-Lena-Estrada *et al.*, 2021), to compute the elastic properties of shale rock samples from diverse geological origins (Nicolás-López *et al.*, 2019) and, to estimate attenuation effects and dispersion of velocities on sandstones saturated with brine (Valdiviezo-Mijangos *et al.*, 2020).

The ternary mineral RPTs that we used here to study the AND-2A drillcore were built in terms of the elastic properties of mixed clays, quartz, and calcite. We chose these minerals because the AND-2A drillcore mainly contains siliciclastic sediments consisting of diamictite [a poorly sorted sedimentary rock, characteristic of glacial sediments that contain clasts of various sizes ranging from clay to boulders embedded in either a sand or mud matrix], sandstones, and mudstones which are cemented by calcareous minerals (Fielding *et al.*, 2008; Hunze *et al.*, 2013; Iacoviello *et al.*, 2015). Furthermore, smectite and illite are the main clay minerals present along the drillcore with a minor presence of kaolinite and chlorite (Iacoviello *et al.*, 2012). We also consider that the rock's porous space is brine saturated. As such, brine is considered as an inclusion form.

In the next section, a summary of the SC method is first given, followed by a description of the methodology used to obtain the core logging data from the AND-2A drillcore. Results are then compared to the lithology interpreted from the implementation of Gardner-type density-velocity cross plots (Gardner *et al.*, 1974). Results from SC and Gardner methods are also compared to the lithology reported by Fielding *et al.* (2008) and with the visual description of six selected rock specimens that were trimmed off the AND-2A drillcore at different depths.

METHODS

SELF-CONSISTENT METHOD

In the SC scheme proposed by Sabina and Willis (1988), the effective elastic properties of the AND-2A drillcore such as both the bulk and the shear moduli, κ_{eff} and μ_{eff}, and the wet bulk density ρ_{WBDeff} can be modelled using the following equations:

$$\kappa_{eff} = \kappa_{n+1} + \sum_{r=1}^{n} \frac{\alpha_r \left(\kappa_r - \kappa_{n+1} \right)}{1 + 3 \left(\kappa_r - \kappa_{eff} \right) / \left(3\kappa_{eff} + 4\mu_{eff} \right)}, \tag{1}$$

$$\mu_{eff} = \mu_{n+1} + \sum_{r=1}^{n} \frac{\alpha_r \left(\mu_r - \mu_{n+1} \right)}{1 + 6 \left(\mu_r - \mu_{eff} \right) \left(\kappa_e + 2\mu_{eff} \right) / \left[5\mu_{eff} \left(3\kappa_{eff} + 4\mu_{eff} \right) \right]}, \tag{2}$$

$$\rho_{WBDeff} = \rho_{n+1} + \sum_{r=1}^{n} \alpha_r \left(\rho_r - \rho_{n+1} \right). \tag{3}$$

In equations (1) through (3), κ_{n+1}, μ_{n+1} and ρ_{n+1} are respectively both the bulk and shear moduli and the density of the mineral matrix while the bulk modulus, the shear modulus, the density and the volume fraction for a given inclusion r are represented by κ_r, μ_r, ρ_r and α_r where $r=1,2,…,n$. If the volume fraction of the mineral matrix is represented by α_{n+1}, then it follows that

$$\sum_{r=1}^{n+1} \alpha_r = 1. \tag{4}$$

Later, equation (4) can be rewritten as follows: $\sum_{r=1}^{n+1} \alpha_r = \alpha_r^{sol} + \alpha_r^{fl} = \alpha_r^{sol} + \phi = 1$, where both the volume fraction of the solids (minerals) and the pore fluid are respectively represented by α_r^{sol} and α_r^{fl}. For instance, ϕ is the void fraction of the rock that is saturated with fluid. As above mentioned, in this work, the solids are represented by mixed clays, quartz, and calcite while the saturating fluid is brine. In the SC approach, the matrix can be represented by any of these three main minerals. Thus, when any one of these minerals acts as the matrix, the other two remaining minerals and the brine act as the inclusions. The physical properties of the minerals and the brine used as input data in equations (1) through (3) are shown in Table 1 (Mavko *et al.*, 2009). These equations can be easily implemented using any encoding software. However, equations (1) and (2) must be iteratively solved. Lizcano-Hernández *et al.* (2018) and López-Lena-Estrada *et al.* (2021) portray flowcharts that explain the solution of these equations using the fixed point technique. Therefore, V_{peff} can be simply estimated as $V_{peff} = \left(\dfrac{K_{eff} + \mu_{eff}}{\rho_{WBDeff}} \right)^{1/2}$.

Table 1. Physical properties of the minerals and the fluid used as input in the SC modelling (Mavko et al., 2009): * values for mixed clays, ** values calculated at atmospheric pressure, at 20 °C and 3.5% salinity.

Mineral or fluid	ρ_r [gr/cm³]	Vp_r [km/s]	Vs_r [km/s]
Clays	2.6*	3.41*	1.63*
Quartz	2.65	6.05	4.09
Calcite	2.71	6.64	3.44
Brine	1.02**	1.52**	------

AND-2A DRILLCORE SETTINGS: PHYSICAL CHARACTERISTICS

Core logging data includes the wet bulk densities ρ_{WBD} and the compressional wave velocities V_p that were estimated with the Geotek Multi-Sensor Core-Logger (MSCL) system [http://www.geotek.co.uk/].

Compressional travel times were measured across the core diameter by leading the AND-2A drillcore through a couple of pulser-receiver P-wave Acoustic Roller Contact (ARC) piezo-electric ceramic transducers (230 kHz of central frequency). The core diameter was determined by the displacement

of the acoustic rollers as they travelled over the core. This technique allows the estimation of V_p profiles by dividing the measured travel times by the measured core diameter [see Dunbar *et al.* (2009) for additional details].

Then, a pair of ^{137}Cs gamma-ray γ source and detector mounted across the drillcore provide a core wet bulk density ρ_{WBD} profile. Briefly, gamma rays travelling through the composite lose energy as they are dispersed by the electrons present in the medium. The latter leads to the detected radiation being diminished. This energy loss can be associated with the density of the electrons ρ_e that correspond to the detected gamma-ray beam as follows:

$$\rho_e = 2\rho_{WBD} \frac{Z}{A}, \tag{5}$$

where the atomic number Z and the molecular weight A of the medium can be taken as $\frac{Z}{A} = \frac{1}{2}$ with negligible error for most rocks (Keller, 1988).

RESULTS AND DISCUSSION

Figure 1(a) portrays density-velocity ternary mineral RPTs built by using the SC method. In these RPTs, the upper triangle is representative of a solid heterogeneous rock $\alpha_r^{fl} = \phi = 0\%$ which vertices are defined as CL100% (clay), CA100% (calcite) and QR100% (quartz) while the vertices of the modelled triangles with brine (BR) filling void fractions of 20% and 40% are defined as BR20%+CL80%, BR20%+CA80% and BR20%+QR80%; and BR40%+CL60%, BR40%+CA60% and BR40%+QR60% respectively.

Figure 1(b) displays the full AND-2A drillcore log data overlapped on the ternary mineral RPTs shown in Figure 1(a). Our mineral lithotype interpretation is carried out in terms of the areas related to the elastic responses of the minerals. In this sense, we identify in Figure 1(b) the following mineral lithotypes: argillaceous lithotype, clay-rich siliceous lithotype and siliceous lithotype (Gamero-Diaz *et al.*, 2013). Note that the contribution of calcite to the observed elastic properties of the drillcore is negligible, as also pointed out by Staudigel *et al.* (2018) where calcite was found to be a rare constituent of the lithology of the AND-2A instead of occasionally appearing as veins or pore-filling cement.

Also, note that, while mineral ternary diagrams attempt to model the AND-2A drillcore's elastic response considering the presence of mixed clays, quartz and calcite, the data points lying outside the ternary mineral RPTs could indicate intervals with the presence of minerals whose elastic properties may be significantly different from mixed clays, quartz and calcite, since most rocks are made up of more than three dominant minerals. However, observed high V_p (≥ 4.5 km/s) and ρ_{WBD} (≥ 2.6 gr/cm³) in glacial sediments can also be related to the existence of large lonestones (Niessen & Jarrard, 1998; Niessen *et al.*, 1998).

Figure 2 portrays a log density- log velocity cross plot showing the lithotype interpretation of the AND-2A drillcore data carried out by using the relationship between density (ρ) and compressional velocity (V_p) proposed by Gardner (Gardner *et al.*, 1974)

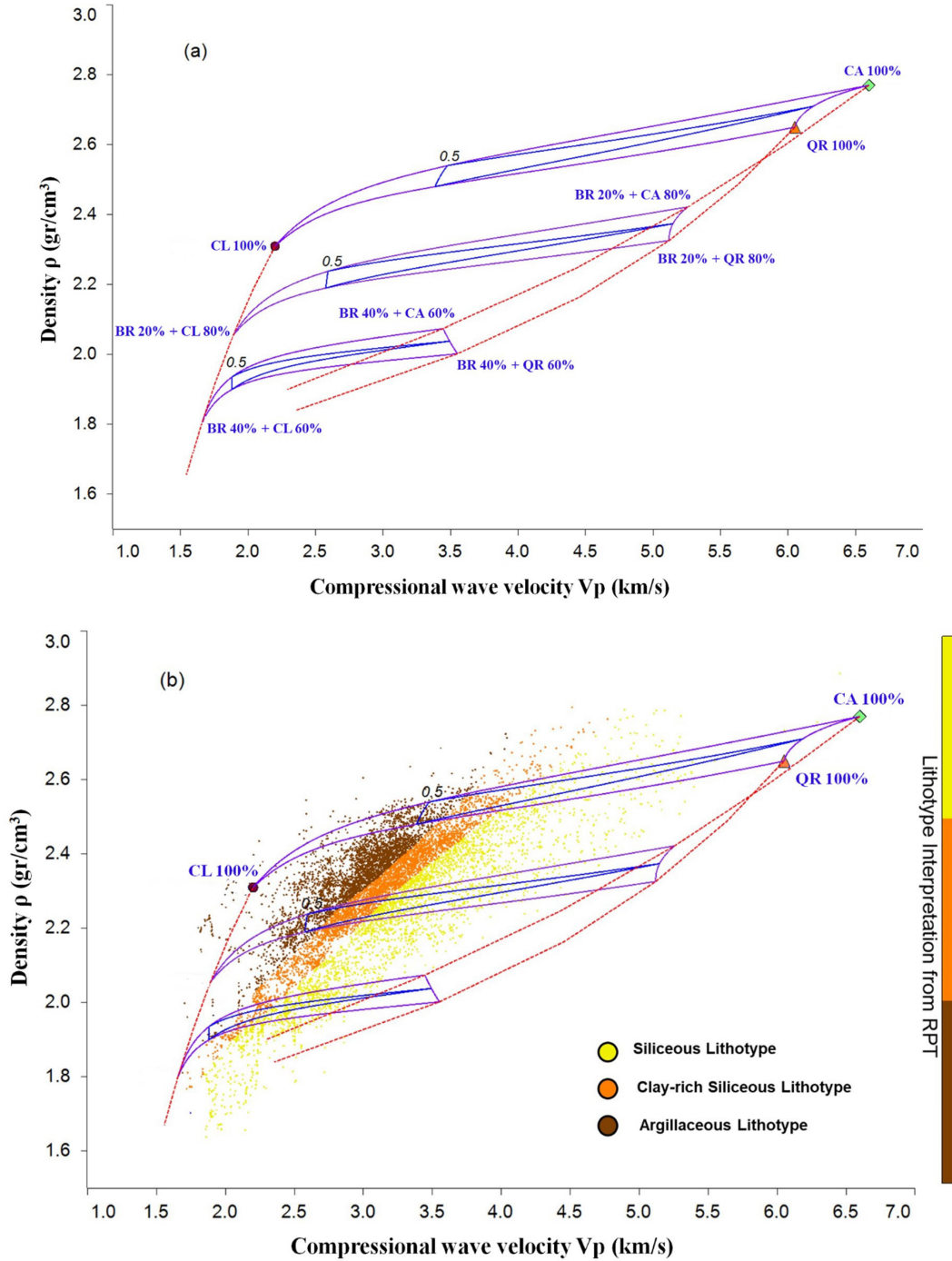$$\rho = \alpha V_P^{0.25}. \tag{6}$$

Figure 1 (a). Density - velocity ternary mineral RPTs built from the SC approach to model the AND-2A drillcore's elastic response. These RPTs integrate the mineralogy and the brine saturation at 0%, 20% and 40% void fractions resulting in vertices for the upper triangle defined as CL100% (clay), CA100% (calcite), and QR100% (quartz) while the vertices of the middle and lower triangles are defined as BR20%+CL80%, BR20%+CA80% and BR20%+QR80%; and BR40%+CL60%, BR40%+CA60% and BR40%+QR60% respectively. (b) AND-2A drillcore's mineral lithotype interpretation using the RPT portrayed in Figure 1(a). The volume fractions corresponding to the vertices of middle and lower are not shown to improve visualization of the data points. The lithotype zones are related to the mineral elastic response. Three mineral lithotypes are identified: argillaceous lithotype, clay-rich siliceous lithotype and siliceous lithotype.
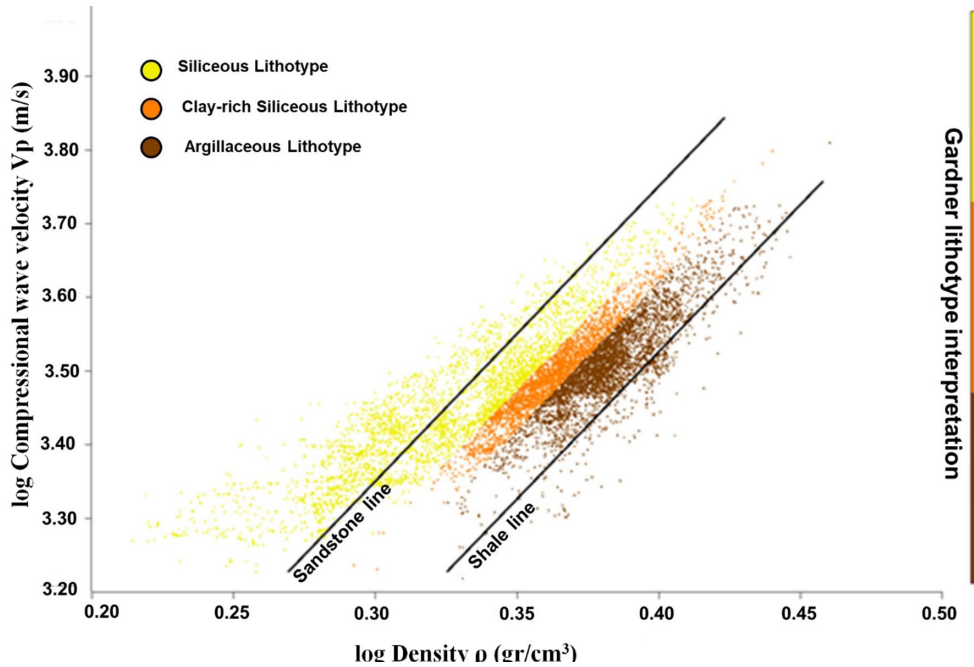
Figure 2. Lithotype interpretation of the AND-2A Drillcore by using Gardner type density-velocity cross plots. This figure shows the shale line, $\rho = 1.75 V_P^{0.25}$, which defines points with high clay content, while the sandstone line, $\rho = 1.66 V_P^{0.25}$ represents points with high quartz content. In this image, three mineral lithotypes are also identified: argillaceous lithotype, clay-rich siliceous lithotype and siliceous lithotype.

Typical values for coefficient α are α = 1.66 for sandstones and α = 1.75 for shales (Mavko *et al.*, 2009). Thus, the shale line, $\rho = 1.75 V_P^{0.25}$, defines trend points for argillaceous lithotypes, while the sandstone line, $\rho = 1.66 V_P^{0.25}$, represents trend points for siliceous lithotypes. Therefore, the clay-rich siliceous lithotype represents the clay to quartz content transition. Figure 3 displays the mineral lithotype sequences obtained from the interpretation of the elastic response in Figures 1(b) and 2. In the AND-2A drillcore the argillaceous lithotype indicates the presence of a variety of argillaceous rocks such as muddy diamictite, mudstone, and claystone while the clay-rich siliceous lithotype is related to clay-rich siltstones. On the other hand, the siliceous lithotype is associated with siliceous rocks, mainly including sandy diamictite, sandstone and sandy conglomerate. Table 2 shows results from Figure 3 compared to the main lithological features corresponding to the LSU's reported by Fielding *et al.* (2008). These LSUs, as portrayed in Figure 3, cover fourteen depth intervals [mbsf] along the AND-2A [also, LSU 8 is divided into four sub-units]. However, the lithological description of the first LSU [0 – 37.7 mbsf] is not included in our work due to the lack of data on this depth interval.

Figures 4 and 5 present photographs and thin sections of six selected samples obtained from the AND-2A. These samples are labelled in terms of the depth interval [mbsf] where they were located and they were chosen as being representative of the fine to coarse grain textures found along the three different geological ages of the AND-2A Drillcore (Acton *et al.*, 2008): lower Miocene (1138.54 to 800 mbsf), middle Miocene (800 to 223 mbsf), and upper Miocene to more recent intervals (223 to 0.0 mbsf). Table 3 shows the lithological visual description of these samples compared to the lithological features obtained from the SC and Gardner methods. Qualitative X-Ray Diffraction (XRD)
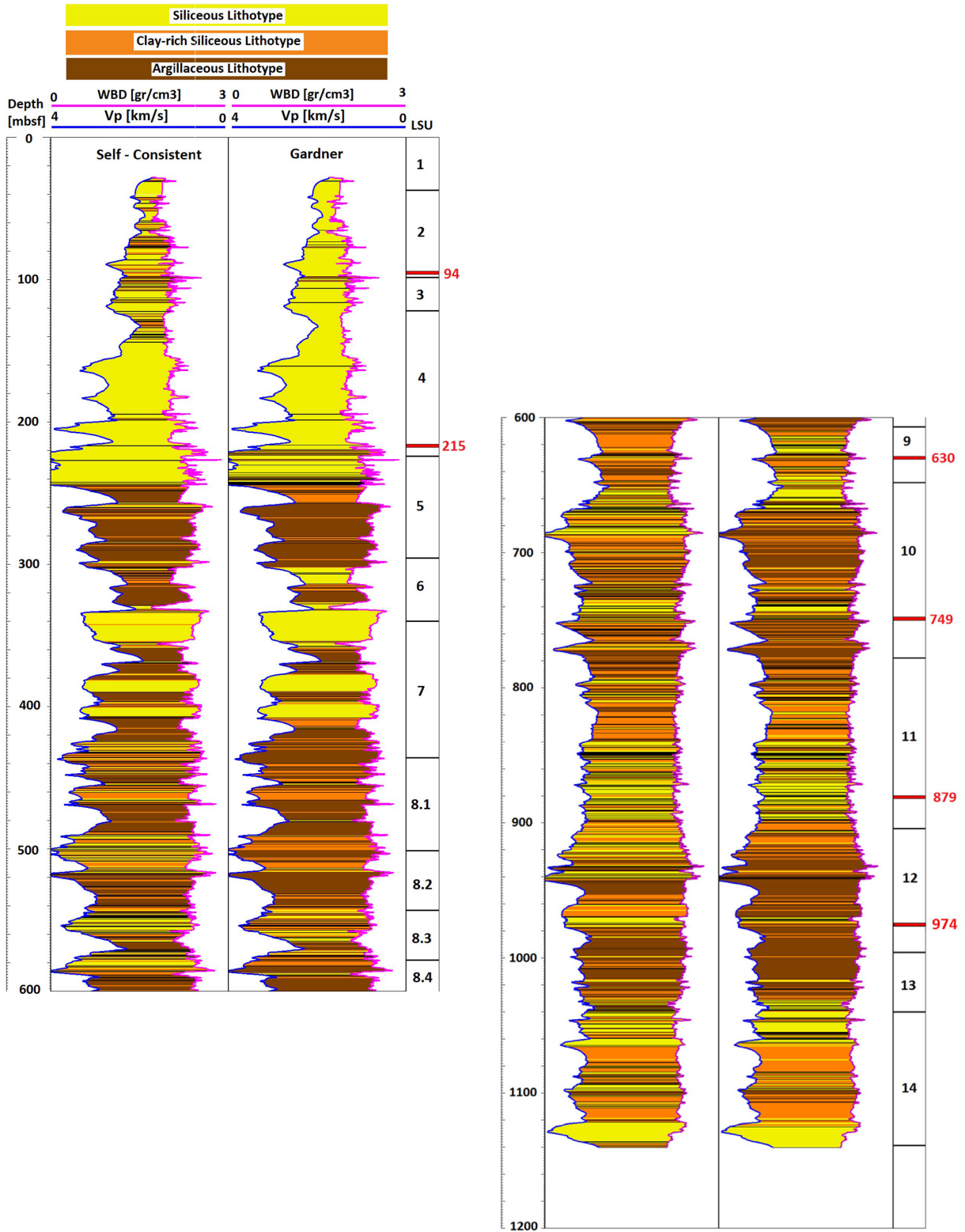
Figure 3. This figure shows the mineral lithotype sequences of the AND-2A drillcore identified from the interpretation of Figures 1 (b) and 2 along with the depth intervals related to the fourteen LSUs covering the AND-2A. The red markers indicate theposition in depth of the six selected samples.

Table 2. The lithological description of the AND-2A obtained from SC and Gardner methods compared to the main lithologies along the LSUs reported by Fielding *et al.* (2008).

| LSU	Depth interval (mbsf)	Lithologies		
		Self-Consistent	Gardner	Fielding et al 2008
2	37.07 – 98.47	Mainly siliceous rocks with interbedded clay-rich siltstones and argillaceous rocks	Mainly siliceous rocks with the sparse presence of clay-rich siltstones and argillaceous rocks	Sandy diamictite interbedded with sandstone, siltstone and sandy conglomerate
3	98.47 – 122.86	Mainly siliceous rocks with interbedded clay-rich siltstones and argillaceous rocks	Mainly siliceous rocks with the sparse presence of clay-rich siltstones and argillaceous rocks	Sandstone and sandy conglomerate
4	122.86 – 224.82	Mainly siliceous rocks with intervals containing clay-rich siltstones and argillaceous rocks	Mainly siliceous rocks	Sandy to silty diamictite, sandstone and siltstone
5	224.82 – 296.34	Argillaceous rocks and minor siliceous rocks	Argillaceous rocks with minor siliceous rocks and clay-rich siltstones	Muddy and sandy diamictite, sandstone
6	296.34 – 339.92	Argillaceous rocks and siliceous rocks with minor clay-rich siltstones	Argillaceous rocks and siliceous rocks with minor clay-rich siltstones	Muddy diamictite, fine-grain sandstone, siltstone and claystone
7	339.92 – 436.18	Siliceous rocks and argillaceous rocks with minor clay-rich siltstones	Siliceous rocks and argillaceous rocks with minor clay-rich siltstones	VB sandy diamictite and volcanic-bearing sandstone
8.1	436.18 – 502.69	Interbedded sequences of argillaceous rocks, siliceous rocks and clay-rich siltstones	Argillaceous rocks interbedded with clay-rich siltstones	VB mudstone, sandstone and muddy diamictite
8.2	502.69 – 544.47	Interbedded sequences of argillaceous rocks, siliceous rocks and clay-rich siltstones	Argillaceous rocks interbedded with clay-rich siltstones	VB muddy diamictite, mudstone and sandstone
8.3	544.47 – 579.33	Siliceous rocks interbedded with argillaceous rocks and clay-rich siltstones	Siliceous rocks interbedded with argillaceous rocks and clay-rich siltstones	VB sandstone, mudstone and sandy diamictite
8.4	579.33 – 607.35	Siliceous rocks and argillaceous rocks interbedded with clay-rich siltstones	Argillaceous rocks with minor presence of limestone	VB muddy diamictite, siltstone and sandstone
9	607.35 – 648.74	Mainly clay-rich siltstones with minor presence of siliceous rocks and argillaceous rocks	Mainly siliceous rocks and clay-rich siltstones	VB sandstone and siltstone
10	648.74 – 778.34	Interbedded sequences of argillaceous rocks, siliceous rocks and clay-rich siltstones	Mainly argillaceous rocks, limestones and minor presence of siliceous rocks	VB sandy diamictite, silty sandstone and mudstone
11	778.34 – 904.66	Mainly siliceous rocks and clay-rich siltstones with a minor presence of argillaceous rocks	Mainly siliceous rocks and clay-rich siltstones with a minor presence of argillaceous rocks	Sandy siltstone and sandstone
12	904.66 – 996.69	Interbedded sequences of siliceous rocks and clay-rich siltstones with minor argillaceous rocks	Prevalence of argillaceous rocks interbedded with clay-rich siltstones. Minor presence of siliceous rocks	Sandy diamictite, silty sandstone and mudstone
13	996.69 – 1040.28	Mainly argillaceous rocks interbedded with siliceous rocks and clay-rich siltstones	Mainly argillaceous rocks and with minor presence of clay-rich siltstones and sands	Siltstone, sandy mudstone and muddy sandstone
14	1040.28 - 1138.54	Prevalence of clay-rich siltstones and siliceous rocks	Prevalence of clay-rich siltstones and siliceous rocks	Sandy diamictite and sandstone
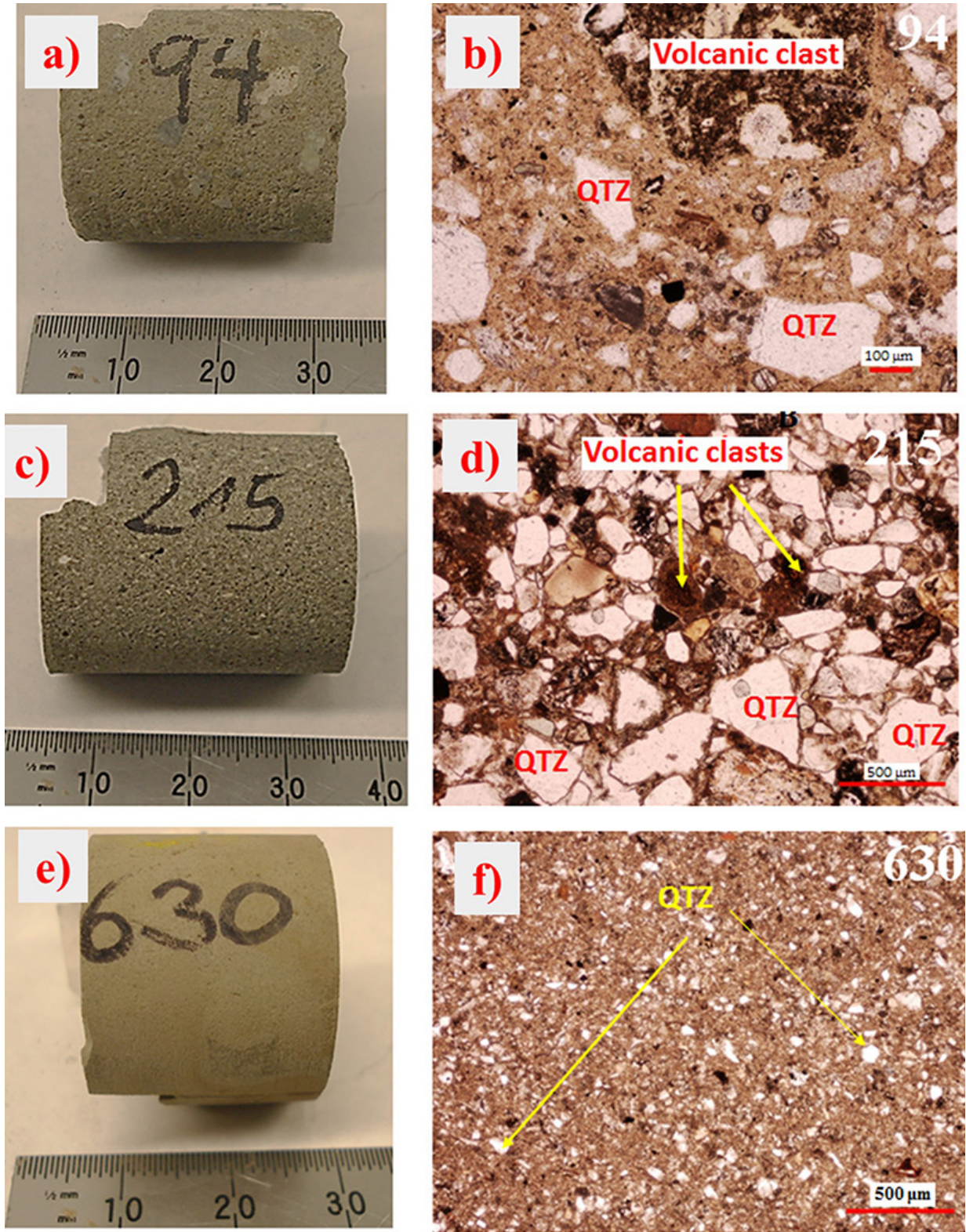
Figure 3. This figure shows the mineral lithotype sequences of the AND-2A drillcore identified from the interpretation of Figures 1 (b) and 2 along with the depth intervals related to the fourteen LSUs covering the AND-2A. The red markers indicate theposition in depth of the six selected samples.
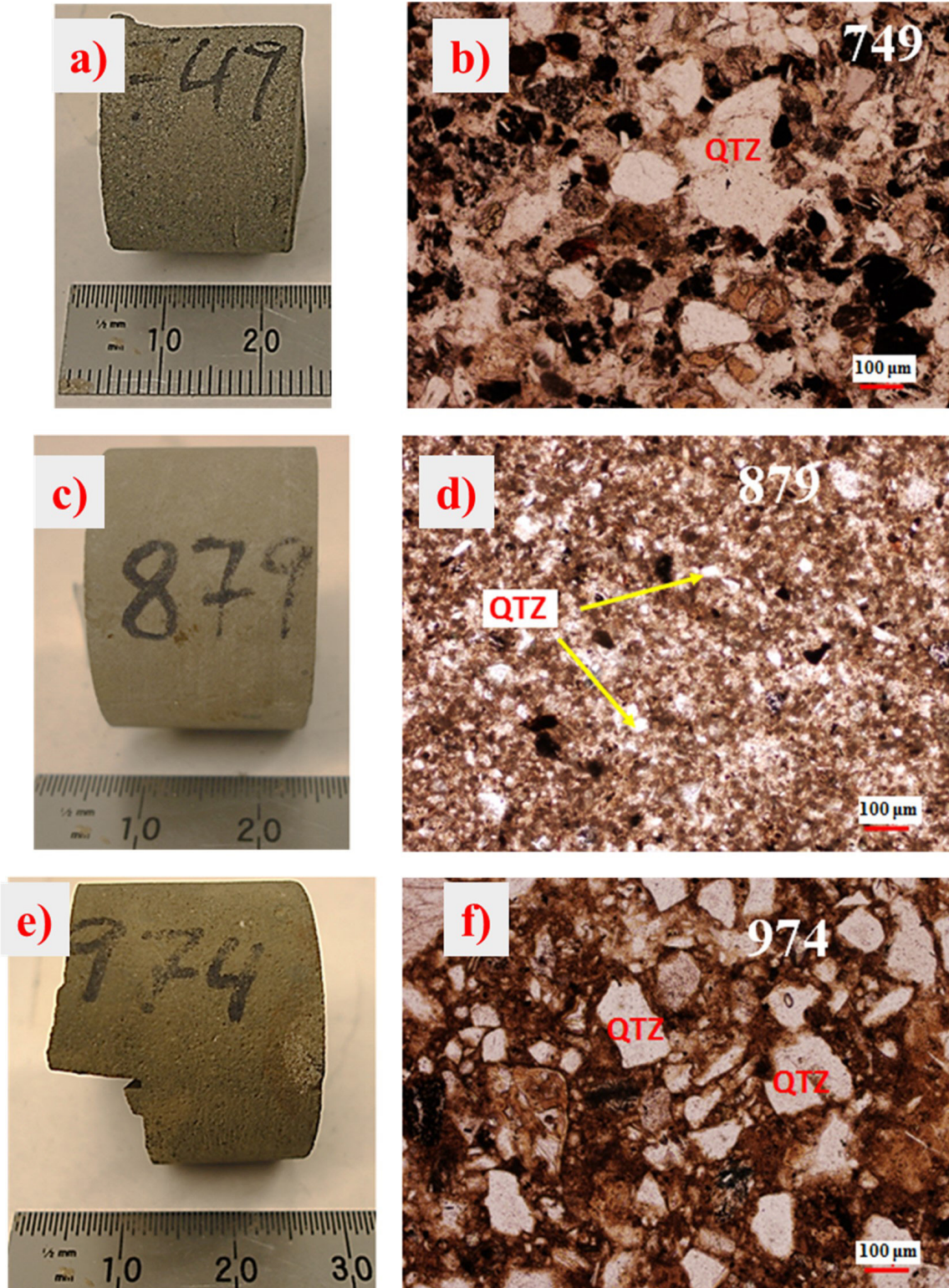
Figure 4. a) Photograph and b) thin section of sample 94: This sample is identified as a sandy diamictite. Quartz minerals (QTZ) and volcanic clasts are shown embedded in a silty matrix. c) Photograph and d) thin section of sample 215: This sample mainly contains coarse sandstone with a minor presence of finer volcanic clasts. c) Photograph and d) thin section of sample 630: identified lithology corresponds to siltstone.

analysis of these samples (see Table 4) show that their constituents minerals are quartz, clay minerals (illite and smectite), carbonates (siderite), calcium minerals (Phillipsite-Ca, Anorthite), feldspars (Orthoclase, Albite, Sanidine, Microline) and mica (muscovite).

From Tables 2 and 3, we can note that the reported lithology from both Fielding *et al.* (2008) and the six selected samples are consistent with the mineral lithotypes obtained from the SC and Gardner methods. Thus, siliceous rocks and clay-rich siliceous rocks (sandy diamictite, sandstone, siltstone) are prevalent in LSU 2 (37.07 – 98.47 mbsf), LSU 3 (98.47 – 122.86 mbsf) and LSU 4 (122.86 – 224.82 mbsf). These mineral lithotypes are also consistent with the lithology of samples 94 (sandy diamictite with a silty matrix) and 215, (coarse sandstone). On the other hand, LSU 5 (224.82 – 296.34 mbsf) and LSU 6 (296.34 – 339.92 mbsf) represent a transition from siliceous rocks to both argillaceous rocks and clay-rich siltstones, while siliceous rocks (mainly sandstones) are characteristic of LSU 7 (339.92 - 436.18 mbsf). LSU 8.1 (436.18 – 502.69 mbsf) and LSU 8.2 (502.69 – 544.47 mbsf) are dominated by argillaceous rocks and siliceous rocks (Volcanic-Bearing VB mudstone, sandstone, and muddy diamictite). However, LSU 8.3 (544.47 – 579.33 mbsf) and LSU 8.4 (579.33 – 607.35 mbsf) are mainly comprised of siliceous rocks (sandstones, sandy diamictite). A finer lithology arises at LSU 9 (607.35 – 648.78 mbsf) consisting of clay-rich siltstone and sandstone with minor mudstones. The lithology of sample 630, a clay-rich siltstone, agrees with these findings. Then, an assemblage of argillaceous rocks, siliceous rocks, and clay-rich siltstones were found in LSU 10 (648.74 – 778.34 mbsf). Indeed, sample 749, Figures 5(a) and 5(b), a silty sandstone, is identified as a combination of clay-rich siltstone and a siliceous rock in Table 3. The LSU 11 (778.34 – 904.66 mbsf) mainly comprises siliceous rocks and clay-rich siltstones (sandy siltstone and sandstone). This lithology also agrees with the lithology of sample 879, a fine grain sandstone. LSU 12 (904.66 - 996.69 mbsf) contains interbedded sequences of clay-rich siltstones with minor mudstones. In particular, the lithology of sample 974, a silty sandstone, is related to the siliceous lithotype as portrayed in Figure 3. LSU 13 (996.69 – 1040.28 mbsf) shows a finer grain lithology than the previous LSU 12. In LSU 13, argillaceous rocks interbedded with clay-rich siltstones are prevalent. On the contrary, coarser grain lithologies such as siliceous rocks and clay-rich siltstones are present in LSU 14 (1040.28 – 1138.54 mbsf).

CONCLUSIONS

We have implemented a micromechanical SC modelling to generate density-velocity rock physics templates for the determination of mineral lithotypes on the AND-2A drillcore. Results show that calcite is an uncommon component of the lithology in the AND-2A as also reported by Staudigel *et al.* (2018). Instead, the identified mineral lithotypes correspond to the argillaceous lithotype, the clay-rich siliceous lithotype and the siliceous lithotype.

On the other hand, the mineral lithotype distribution identified by the ternary mineral RPT's along the AND-2A drillcore is consistent with the interpretation that we obtained from the implementation of Gardner's relationship. These results are also consistent with the main lithological features reported by Fielding *et al.* (2008). Furthermore, the lithology of the six selected samples can be directly correlated with the modelled mineral lithotypes. However, since these results attempt to assist in the characterization of glacial sediments, a more robust interpretation should include petrophysical and stratigraphic studies based on resistivity, neutron porosity, and gamma-ray borehole measurements which are commonly used to discriminate lithology. However, resistivity, neutron

Table 3. Lithology from visual description, SC and Gardner methods of six selected samples cut at different depths along the AND-2A.

Sample	Depth interval (mbsf)	Lithology		
		Description	Self-Consistent	Gardner
94	94.16-96.41	Sandy diamictite with a silty matrix	Siliceous rocks, clay-rich siltstone	Siliceous rocks
215	215.48-215.57	Coarse sandstone	Siliceous rocks	Siliceous rocks
630	628.81-630.89	Sandy mudstone (siltstone)	Clay-rich siltstone	Clay-rich siltstone
749	747.45-749.9	Silty Sandstone	Siliceous rocks, clay-rich siltstone	Siliceous rocks, clay-rich siltstone
879	879.41-879.58	Fine-grain sandstone	Siliceous rocks	Siliceous rocks
974	974.1-975.42	Silty sandstone	Siliceous rocks	Clay-rich siltstone

Table 4. Mineral identification from XR.

Sample (mbsf)	Quartz	Illite	Smectite	Siderite	Phillipsite-Ca	Anorthite	Orthoclase	Albite	Sanidine	Microline	Muscovite
94	X	X		X		X					
215	X			X			X				
630	X	X				X		X			X
749	X		X	X			X	X			
879	X	X		X					X		
974	X	X			X			X	X	X	X

porosity, and gamma-ray data sets are less commonly available than density and velocity data sets. In this sense, the main advantage of RPT's generated from SC modelling is that this approach can be used to identify mineral lithotypes in glacial formations merely from the rock's elastic properties. In addition, any other combination of three minerals can be used. This is particularly useful since the physical properties of a variety of minerals are readily available in scientific literature.

Nevertheless, these results, as presented here, have the potential to add valuable information to the record of Antarctic glacial and geological history obtained from the AND-2A since variations in lithology can be used to describe paleoenvironmental and paleoclimatic changes as well as to identify source rocks (Iacoviello *et al.*, 2012).

ACKNOWLEDGEMENTS

REFERENCES

Acton G., J. Crampton, G. Di Vincenzo, C. R. Fielding, F. Florindo, M. Hannah, D. M. Harwood, S. Ishman, K. Johnson, L. Jovane, R. Levy, B. Lum, M. C. Marcano, S. Mukasa, C. Ohneiser, M. Olney, C. Riesselman, L. Sagnotti, C. Stefano, E. Strada, M. Taviani, E. Tuzzi, K. L. Verosub, G. S. Wilson, M. Zattin and ANDRILL-SMS Science Team. 2008. Preliminary integrated chronostratigraphy of the AND-2A core, ANDRILL Southern McMurdo Sound project, Antarctica. *Terra Antartica*, 15, 211-220.

Brink J. and R. D. Jarrard. 1998. Petrophysics of core plugs from CRP-1 drillhole, Victoria Land Basin, Antarctica. *Terra Antartica*, 5 (3), 291-297

Close D., M. Perez, B. Goodway and G. Purdue. 2012. Integrated workflows for shale gas and case study results for the Horn River Basin, British Columbia, Canada. *The Leading Edge*, 31, 556-569.

Dunbar G. B., C. Atkins, D. Magens and F. Niessen. 2009. Physical properties of the AND-2A core, ANDRILL Southern McMurdo Sound Project, Antarctica. *Terra Antartica*, 15, 49-56.

Fielding C. R., C. B. Atkins, K. N. Bassett, G. H. Browne, G. B. Dunbar, B. D. Field, T. D. Frank, L. A. Krissek, K. S. Panter, S. Passchier, S. F. Pekar, S. Sandroni, F. Talarico and The ANDRILL-SMS Science Team. 2008. Sedimentology and stratigraphy of the AND-2A core, ANDRILL Southern McMurdo Sound Project, Antarctica. *Terra Antartica*, 15, 77-112.

Florindo F., D. Harwood, F. Talarico, R. Levy and The ANDRILL-SMS Science Team. 2008-2009. Background to the ANDRILL Southern McMurdo sound project, Antarctica. *Terra Antartica*, 15, 13-20.

Gamero-Diaz H., C. K. Miller and R. Lewis. 2013. sCore: A Mineralogy Based Classification Scheme for Organic Mudstones. SPE Annual Technical Conference and Exhibition. Society of Petroleum Engineers New Orleans, Louisiana, USA.

Gardner G. H. F., L. W. Gardner and A. R. Gregory. 1974. Formation velocity and density—the diagnostic basics for stratigraphic traps. *Geophysics*, 39, 770-780.

Hunze S., H. Schröder, G. Kuhn and T. Wonik. 2013. Lithostratigraphy determined from downhole logs in the AND-2A borehole, southern Victoria Land Basin, McMurdo Sound, Antarctica. *Geosphere*, 9, 63-73.

Iacoviello F., G. Giorgetti, F. Nieto and I. T. Memmi. 2012. Evolution with depth from detrital to authigenic smectites in sediments from AND-2A drill core (McMurdo Sound, Antarctica). *Clay Minerals*, 47, 481-498.

Iacoviello F., G. Giorgetti, I. Turbanti Memmi and S. Passchier. 2015. Early Miocene Antarctic glacial history: new insights from heavy mineral analysis from ANDRILL AND-2A drill core sediments. *International Journal of Earth Sciences*, 104, 853-872.

Keller G. V. 1988. A practical introduction to borehole geophysics. *EOS Transactions*, 69, 850-851.

Lizcano-Hernández E. G., R. Nicolás-López, O. C. Valdiviezo-Mijangos and J. Meléndez-Martínez. 2018. Estimation of brittleness indices for pay zone determination in a shale-gas reservoir by using elastic properties obtained from micromechanics. *J. Geophys. Eng.*, 15, 307-314.

López-Lena-Estrada A., J. Meléndez-Martínez, O. C. Valdiviezo-Mijangos and R. Nicolás-López. 2021. Design and development of a robust computing workflow to build rock physics templates from a micromechanical self-consistent model. *J Appl Geophys*, 184, 104248.

Mavko G., T. Mukerji and J. Dvorkin. 2009. The Rock Physics Handbook: Tools For Seismic Analysis Of Porous Media. New York: Cambridge University Press.

Nicolás-López R., J. Meléndez-Martínez, A. López-Lena-Estrada, O. C. Valdiviezo-Mijangos, C. Couder-Castañeda, E. Coconi-Morales and J. A. España-Pinto. 2020. Micromechanics modelling for mineral volume fraction determination: application on a terrigenous formation. *Scientific Reports*, 10, 16629.

Nicolás-López R. and O. C. Valdiviezo-Mijangos. 2016. Rock physics templates for integrated analysis of shales considering their mineralogy, organic matter and pore fluids. *J. Petrol. Sci. Eng.*, 137, 33-41.

Nicolás-López R., O. C. Valdiviezo-Mijangos, J. Meléndez-Martínez and V. M. Levin. 2019. A multimineral Rock Physics Template built from the Perfectly Disordered Method for shale lithology interpretation. *J. Petrol. SCi. Eng.*, 176, 532-536.

Niessen F. and R. D. Jarrard. 1998. Velocity and porosity of sediments from CRP-1 drillhole, Ross Sea, Antarctica *Terra Antartica*, 5 (3), 311-318

Niessen F., R. D. Jarrard and C. Bücker. 1998. Log-based physical properties of the CRP-1 Core, Ross Sea, Antarctica. *Terra Antartica*, 5 (3), 299-310

Sabina F. J. and J. R. Willis. 1988. A simple self-consistent analysis of wave propagation in particulate composites. *Wave Motion*, 10, 127-142.

Staudigel P. T., S. Murray, D. P. Dunham, T. D. Frank, C. R. Fielding and P. K. Swart. 2018. Cryogenic brines as diagenetic fluids: Reconstructing the diagenetic history of the Victoria Land Basin using clumped isotopes. *Geochimica et Cosmochimica Acta*, 224, 154-170.

Stephenson D. A., A. H. Fleming and D. M. Mickelson. 1988. Glacial deposits. In: W. Back, J. S. Rosenshein and P. R. Seabers (eds.). Hydrogeology: The Geology of North America. Geological Society of America pp. 301-314.

Valdiviezo-Mijangos O. C., J. Meléndez-Martínez and R. Nicolás-López. 2020. Self-consistent and squirt flow modelling of velocity dispersion and attenuation for effective-stress dependent experimental data. *Explor. Geophys.*, 51, 248-255.

Valdiviezo-Mijangos O. C. and R. Nicolás-Lopez. 2014. Dynamic characterization of shale systems by dispersion and attenuation of P-and S-waves considering their mineral composition and rock maturity. *J. Petrol. Sci. Eng.*, 122, 420-427.

Wilson G. S., T. R. Naish, R. D. Powell, R. H. Levy and J. S. Crampton. 2012. Late Neogene chronostratigraphy and depositional environments on the Antarctic Margin: New results from the ANDRILL McMurdo Ice Shelf Project. *Global and Planetary Change*, 96-97, 1-8.

Wonik T., T. Grelle, D. Handwerger, R. D. Jarrard, A. McKee, T. Patterson, T. Paulsen, S. Pierdominici, D. R. Schmitt, H. Schroeder, M. Speece and T. Wilson. 2008-2009. Downhole Measurements in the AND-2A Borehole, ANDRILL Southern McMurdo Sound Project, Antarctica. *Terra Antartica*, 15(1), 57-68.